Published in final edited form as:
Neurobiol Dis. 2009 October ; 36(1): 60–69. doi:10.1016/j.nbd.2009.06.014.

Murine Glut-1 transporter haploinsufficiency: postnatal deceleration of brain weight and reactive astrocytosis

Paivi M. Ullner[a], **Alessia Di Nardo**[d], **James E. Goldman**[b], **Scott Schobel**[c], **Hong Yang**[a], **Kristin Engelstad**[a], **Dong Wang**[a], **Mustafa Sahin**[d], and **Darryl C. De Vivo**[a]

[a]Dept. of Neurology, Colleen Giblin Laboratories for Pediatric Neurology Research, Columbia University, New York, NY, USA

[b]Dept. of Pathology, Columbia University, New York, NY, USA

[c]Dept. of Psychiatry, Columbia University, New York, NY, USA

[d]Dept. of Neurology, Children's Hospital, Harvard Medical School, Boston MA, USA

Abstract

Glucose transporter type 1 (Glut-1) facilitates glucose flux across the blood-brain-barrier. In humans, Glut-1 deficiency causes acquired microcephaly, seizures and ataxia, which are recapitulated in our Glut-1 haploinsufficient mouse model. Postnatal brain weight deceleration and development of reactive astrogliosis were significant by P21 in Glut-$1^{+/-}$ mice. The brain weight differences remained constant after P21 whereas the reactive astrocytosis continued to increase and peaked at P90. Brain immunoblots showed increased phospho-mTOR and decreased phospho-GSK3-β by P14. After fasting, the mature Glut-$1^{+/-}$ females showed a trend towards elevated phospho-GSK3-β, a possible neuroprotective response. Lithium chloride treatment of human skin fibroblasts from control and Glut-1 DS patients produced a 45% increase in glucose uptake. Brain imaging of mature Glut-$1^{+/-}$ mice revealed a significantly decreased hippocampal volume. These subtle immunochemical changes reflect chronic nutrient deficiency during brain development and represent the experimental correlates to the human neurological phenotype associated with Glut-1 DS.

Keywords

Glut-1 deficiency mouse model; brain development; microcephaly; apoptosis; proliferation; astrogliosis; mTOR; GSK3-β; fasting; lithium

INTRODUCTION

Brain depends on glucose as the preferred substrate for energy production. Glucose transporter type 1 (Glut-1) facilitates the diffusion of glucose across the blood-brain-barrier (BBB) (Maher et al., 1994). A deficiency of Glut-1 results in decreased CSF glucose (hypoglycorrhachia) and brain energy failure (De Vivo et al., 1991). The classical features of Glut-1 deficiency syndrome (Glut-1 DS) are acquired microcephaly, infantile seizures, developmental delay, disorders of movement, speech and language impairment, and cognitive impairment. GLUT-1 haploinsufficiency is the result of more than 60 different pathogenic mutations (Wang et al., 2005). The children are normal at birth, and develop symptoms post-natally. The clinical severity of the neurological phenotype varies from severe to minimal. Also, the degree of

Corresponding Author: Darryl C De Vivo, MD, Neurological Institute, 710 W 168 Street, Room 201, New York, NY, USA 10032 dcd1@Columbia.edu.

acquired microcephaly varies from one patient to another with a few patients experiencing normal growth. The pathophysiology underlying the symptoms remains obscure. There is essentially no available neuropathology since the condition is not life-threatening.

We previously reported a haploinsufficient Glut-1 mouse model (Glut-$1^{+/-}$) exhibiting hypoglycorrhachia, decreased brain weight, impaired motor performance, epileptiform discharges on the electroencephalogram and diminished brain glucose metabolism by positron emission tomography. The neuropathology in the mature mice was normal using conventional tissue staining methods. The homozygous Glut-$1^{-/-}$ genotype is embryonic lethal around E11-12 whereas the heterozygous Glut-$1^{+/-}$ embryo develops normally to term (Wang et al., 2006).

Normally, Glut-1 is expressed at the preimplantation stage (Hogan et al., 1991), with Glut-1 localizing to the microvasculature by E11.5 (Daneman et al., 2009). Glut-1 expression remains low during the first post-natal week, increasing to adult levels by the third postnatal week as the suckling pup is weaned (Khan et al., 1999; Vanucci and Simpson, 2003). A link between Glut-1 DS and increased developmental apoptosis has been suggested. Decreased Glut-1 expression enhanced apoptosis in mouse blastocysts (Chi et al., 2000; Heilig et al., 2003). Abrogation of the GLUT1 orthologue in zebrafish is embryonic lethal and simultaneous abrogation of the pro-apoptotic gene, BAD, reverses the effect and permits survival (Jensen et al., 2006).

The AMPK/TSC/mTOR-pathway regulates cell size and survival, and is modulated by cellular energetics, growth factors and stress. Protein translation increases when growth signals phosphorylate Akt, mTOR (mammalian target of rapamycin), downstream kinases (S6K1), and ribosomal S6. (Hay et al., 2004; Yang and Guan, 2007; Hammerman et al., 2004) With energy deprivation, AMP-activated protein kinase is phosphorylated (P-AMPK) conserving energy through mTOR inhibition (Ramamurthy et al., 2006; Hay et al., 2004), and promoting energy availability through fatty acid oxidation via Acetyl-CoA-carboxylase (P-ACC) (Steinberg et al., 2006). Additionally, P-Akt exerts a neuroprotective effect by inactivating glycogen synthase kinase-3-β (P-GSK3-β) (Frame and Cohen, 2001; Endo et al., 2006; Beurel and Jope, 2006). And it also may promote recycling and transporter activity of Glut-1 (Wieman et al., 2006)

Here we describe a detailed analysis of postnatal brain development in heterozygous Glut-$1^{+/-}$ mice. In particular, we investigated postnatal cellular stress, mTOR signaling and cell death in the Glut-$1^{+/-}$ mouse brain as the potential pathophysiologic mechanisms associated with Glut-1 DS.

MATERIALS AND METHODS

Materials

The studies were performed in the Glut-$1^{+/-}$ mouse model that was previously created by deleting the promoter region and exon 1 and inserting the PGK-Neo fusion cassette in the 129S6/SvEvTac mouse background, (Wang et al., 2006, see introduction for further description). A total of 172 female and male Glut-$1^{+/-}$ and 157 wild type (WT) mice between ages P1-720 were sacrificed for the brain weight analysis. A detailed histological and Western blotting analysis was performed at ages P7-21 (N=110), 3-6 months (N=44), 9 months (female N=6), and 21-24 months (female N=7). About 50 litters in total were used in the brain weight studies. The appropriate combination of genotypes was achieved by pooling 3-6 litters for each experiment. The litter size, varying from 3-9 pups, required the pooling of litters to accumulate a sufficient number of animals for each experiment. Before sacrifice, the mice were anesthetized (ketamine 80 mg/kg; xylasine 10 mg/kg ip.). The mice used for histological

analysis underwent transcardial perfusion (0.1M PBS, followed by 4% paraformaldehyde in 0.1 M PBS, pH 7.4). The brains were transected at the base of the medulla, and weighed fresh after removing the olfactory bulb. All weaned mice were allowed free access to regular chow and drinking water, unless otherwise stated as part of a specific experiment. All suckling pups were reared with their dams in their regular physiological environment. All animal procedures were performed in accordance with protocols approved by the Columbia University Institutional Animal Care and Use Committee.

Histology / Immunohistochemistry

The brains were immersed in 4% paraformaldehyde (12 h) and processed for paraffin blocks (6 μm coronal sections) or cryoprotected (30% sucrose, 48 h), frozen in liquid nitrogen in O.C.T. and stored (−80C) until sectioning by Cryostat (10 μm coronal/30 μm axial).

H&E, Nissl, and glial fibrillary acidic protein (GFAP) staining was performed at ages P7-21, 3-6 months, 9 months, and 21-24 months. Luxol fast blue (LFB) staining was performed in the animals older than 9 months. At least three Glut-$1^{+/-}$ animals per age group were compared with their age-matched controls. Representative sections were examined from forebrain, midbrain and hindbrain regions. The histological architecture of these regions was evaluated by the first author (PU) and confirmed by a neuropathologist (JG). We used the Mouse Brain Atlas with stereotactic coordinates by Paxinos G., Franklin K.B. (Academic Press, 2007) to identify the mouse brain regions of interest, and, to ensure uniformity when comparing brain samples from the different experiments

TUNEL immunohistochemistry (TdT-mediated dNTP nick end labeling, ApopTag Apoptosis Detection kit S7110, Chemicon) was evaluated in the female brain specimens at P9, P10, P12, P16, 3 months, and 12 months in all brain regions. TUNEL (+) cells were quantified at P10 (at the time of first detected deceleration of the brain growth) on bilateral hemispheric specimens from cerebrum (Bregma: −0.94…−1.46) and cerebellum (Glut-$1^{+/-}$ N=3-4, WT N=3-4; 4 coronal sections q30μm/ mouse, 8 photographs [10x] / section per region of interest). Similarly, all brain regions were evaluated by phospho-Histone-3 (Upstate Biotech, 1:200) and/ or BrDU (bromodeoxyuridine, BrdU In Situ Detection Kit, BD Biosciences, 100mg/kg, ip., 24 hours before sacrifice) at P2, P7, P10, P12, P16, P30, P60, and 3 months. Cerebellar proliferation was quantified with phospho-Histone-3, and cerebral proliferation (cortical layers 1-3) with BrdU at P10, in slides matched to the TUNEL quantification.

Blinded stereologic neuron counts were performed at P21 (N=8 females each group) on right hippocampus CA1 pyramidal cells and dentate gyrus granular cells (cresyl violet, 30 μm axial sections, 10 sections q120μm/ mouse; optical fractionator settings: 50×50 sq., grid size 100×100, [100x]). We determined the total area that was counted by using the stereologic software (Stereoinvestigator). The cell density was calculated as follows: total number of cells as determined by the stereologic counting procedure/ total counted area. The same stereologic neuron counting procedure was performed in the area of somatosensory cortex (200×800 μm rectangular area in auditory cortex, Allen Brain Atlas (Http://mouse.brain-map.org)) that included layers 1-6 located adjacent to the hippocampal formation (N=4 females each group). The total cortical thickness adjacent to the hippocampal formation was measured in these animals at 4x magnification. A similar stereologic procedure was applied to count neurons in the same brain regions of mature mice (N=7 each group; Glut-$1^{+/-}$ mean age 18 months; WT mean age 14 months). These ages were comparable to the ages of animals in the MRI volumetric analysis studies.

Reactive astrocytosis (GFAP, Vision Biosystems, 1:400) was quantified on somatosensory cortex layer 1-3 and piriform cortex on females at ages of P14, P21, P60, P90, and P270 (9 months) (N=3-4 ea. group; 4 coronal sections at 30 μm intervals, 4-8 bilateral photographs

[40x] / section per region of interest, Bregma: 0.22…−1.58). Astrocytes with clearly identifiable cell bodies were included in the counts.

Somatodendritic compartment was analyzed in 3-4-month-old female mice (N=3-4 ea. group), (when both brain weight deceleration and reactive astrocytosis had stabilized). Neuron size was measured in somatosensory cortex (layers 2-3 and 5) and piriform cortex on SMI-311-neurofilament stained sections (Covance, 1:400). At least 150 neurons per region of interest and only the cells with complete nuclear contour (not touching other cells), were quantified at 40x magnification. Dendritic compartment was further visualized with SMI-32 (Covance, 1:400) and MAP2 (Sigma, 1:400). Dendritic branching and dendritic spines were visualized by Golgi-Cox staining in [40x/100x] 8-bit grayscale pictures (FD Rapid GolgiStain Kit, FD NeuroTechnologies, Inc.), and the number of dendritic branches were quantified (somatosensory cortex layer 5: N=10 neurons ea. group, at intersection of two concentric circle perimeters (r=2 μm / r=4 μm, Image J) drawn around the nucleus). Phospho-S6 (Cell Signaling, 1:300) was analyzed at P10, when the pups were physiologically breastfed, and after 6-hour-fasting in 3-6 month old female and male animals (min. N=4 ea. group). Quantification was done at both ages on female somatosensory cortex layer 5 (WT N=3, Glut-$1^{+/-}$ N=5; 4 coronal sections at 30 μm intervals, 4 unilateral photographs [40x] / section, Bregma: −2.3…−2.7).

Pictures were taken with Nikon Eclipse TE300 microscope, Spot Insight Firewire camera and Spot Advance imaging software. Image J software (U.S. National Institutes of Health, Bethesda MD, USA; http://rsb.info.nih.gov/ij) was used for image processing for quantification and cortical measurement. Stereological neuron counts were done with Stereo Investigator software with optical fractionator technique (West, 1999). Statistical analysis was done with Microsoft Excel.

Western blotting

Female and male mouse brains were collected at P7 and P14 (min N=4 ea. group, suckling pups), and at 3-6 months (Glut-$1^{+/-}$ N=13, WT N=11). Additionally, 5 Glut-$1^{+/-}$ females and 6 Glut-$1^{+/-}$ males were exposed to 6-hour-fasting period, with their age-matched controls, before sacrifice. Brain lysates were immunoblotted for mTOR signaling (tuberin, P-tuberin ^{Thr1462}, hamartin, mTOR, P-mTOR ^{Ser2481}, P-AMPK-α ^{Thr172}, AMPK-α, P-ACC ^{Ser79}, ACC1, LKB1, P-Akt-1^{Ser473}, Akt-1, PS$6^{Ser235/236}$, P-GSK3-β^{Ser9}, GSK3-β, tubulin, Glut-1), apoptosis (total caspase-3, cleaved caspase-3, cleaved PARP-1), and synaptic proteins (synapsin-1, PSD-95).

After harvesting, the brains were frozen in liquid nitrogen, and stored at -80C. The brain protein extracts were lysed [20 mM Tris-Cl pH7.5, 140 mM NaCl, 10 mM of NaF, 1 mM Na3VO4, 1 mM EDTA with 1% Triton X-100, and a protease inhibitor by Sigma] by 20 strokes in a tight-fitting Dounce homogenizer. The lysates were centrifuged (14 000 rpm, 30 min, +4C), supernatants were mixed with SDS buffer, heated to 95°C (5 min), and stored frozen. Equal amounts of protein were verified by Commassie gel staining before discontinuous gel electrophoresis, and then subjected to SDS–PAGE, transferred to Immobilon-P Millipore, and incubated in blocking solution [5% non-fat milk powder in TBS-T at RT for 2 hrs. Primary antibodies (Cell Signaling/ Glut-1: α-Diagnostics) and secondary antibodies were diluted in blocking solution to the appropriate concentrations. Membranes were developed using an ECL system (Boston Bioproducts) followed by exposure to x-ray film (X-Omat AR, Eastman Kodak Co.).

Brain MRI volumetric analysis

Age-matched Glut-$1^{+/-}$ and WT mouse brain (T2-weighted axial MRI images, 10 slices, rostral to dorsal, 0.6 mm slice thickness, 0.1mm slice gap) were quantified for total forebrain, total

cerebellum and total hippocampus volume (N=7 ea. group, mean age 17 months, range 14-24 months). The volume was calculated by using the outline of the morphologic structure of the region of interest using ITK-SNAP (Yushkevich et al., 2006). All imaging was performed with a Bruker AVANCE 400WB spectrometer (Bruker NMR, Billerica, MA, USA), and 9.4 T vertical Bruker magnet (Oxford Instruments, Oxford, UK).

Lithium chloride studies

Glut-1 DS patient (N=5, ea. patient had different mutations: R66F, R93W, R126H, R333W, hemizygous deletion) and healthy parent (N=3) fibroblasts were plated on two 6-well-plates (2 million cells/well) each subject, and were grown to confluence (37C humidified air, 5% CO2; culture media: D-MEM (Gibco), 10% FBS, 1% L-glutamine, 0.5 % penicillin-streptomycin). Before treatment, the cells were rinsed with culture media, and 6 wells per ea. subject were incubated in 1mL culture media + 20mM lithium chloride solution for 24 hours and untreated control plates in 1mL culture media (24h). The cells were washed twice in 1x PBS, incubated for 10 min (2mL, 1xPBS, +37C, pH 7.4), and then incubated in 1 ml Hot/Cold mixture (37C, 10 min, cold 2-DOG (2-deoxy-D-glucose, Sigma); hot 14C 2-DOG, Perkinelmer), and the control wells in 1 ml Hot/Cold mixture with cytochalasin-B (37C, 10 min, Sigma). The radioactive buffer was removed; the reaction stopped with 2 ml stop solution (100μM HgCl2, 10μM Phloretin, 1xPBS), and washed in ice-cold 2 ml 1xPBS three times. 1 ml ice-cold 100% ethanol was added to each well, and the plates were placed on ice for 30 min to extract 2-DOG. The ethanol was transferred to scintillation vials to count DPM. 3×50μm Hot/Cold mixture with cytochalasin, and 3×50μm Hot/Cold mixture without cytochalasin was used to count specific activity. Lysis buffer (0.5 ml, 100 mM NaOH + 0.1% Triton-X-100) was used to digest cells, and protein concentration was determined.

RESULTS

Brain weight and morphology

Glut-$1^{+/-}$ mice did not show any differences in brain weight or body weight compared to WT at P7, P10 or P14 although a trend in deceleration of brain weight was emerging (Table 1.) At P21, Glut-$1^{+/-}$ mice had significantly lower mean brain weight (P=0.001, body weight P=0.2), which was also present in the adult mice (P90-120, P=0.001, body weight P=0.95)). These findings confirm deceleration of brain weight between P7 and P21 in the developing Glut-$1^{+/-}$ mice and no further change in the mature mice. (Figure 1.) The brain MRI volumetric analysis of the mature animals (mean age 17 months) showed a reduced total hippocampal volume in $Glut^{+/-}$ mouse (P=0.02, $Glut^{+/-}$ 206 ± 21, WT 239 ± 23, (mm^3 ± SD)),and a similar, though not significant, trend for decreased volume in forebrain (P=0.1, $Glut^{+/-}$ 2525 ± 106, WT 2650 ± 165), and cerebellum (P=0.3, $Glut^{+/-}$ 517 ± 60, WT 558 ± 75). (Figure 2.)

Glut-$1^{+/-}$ and WT mice at ages P7-21 (N=110), 3-6 months (N=44), 9 months (female N=6), and 21-24 months (female N=7) were analyzed histologically. H&E, Nissl, and LFB staining of cerebral cortex, thalamus, hippocampus, brain stem and cerebellum was normal in Glut-$1^{+/-}$ mice at all postnatal ages examined from 7 days to 24 months. The cortical layering appeared normal, and the cortical thickness was not altered at P21 in Glut-$1^{+/-}$ compared to WT (P=0.15, Glut-$1^{+/-}$ 1.18 mm ± 0.04 SD; WT 1.12 mm ± 0.09 SD). No alterations of hippocampal morphology were detected at any of the ages mentioned above.

Apoptosis

To investigate the mechanism of brain weight deceleration during development, we determined the rate of apoptosis in Glut-$1^{+/-}$ and their WT littermates. Developmental apoptosis (TUNEL), visualized between P9-P16 old mice in the cortex, thalamus, medulla, lateral periventricular areas and cerebellum, was the same in the Glut-$1^{+/-}$ and WT animals. Congruent with these

observations, the western blot did not show increased activation of caspase-3 at P7 or P14 in Glut-$1^{+/-}$ mice compared to WT. Furthermore, we did not detect any signs of enhanced cell death in adult Glut-$1^{+/-}$ animals either by TUNEL staining or by western blotting for cleaved caspase-3 or PARP-1. Quantification (group mean ± SEM) of TUNEL (+) cells at P10, when the brain weight deceleration had already started, showed no differences in cortex (P=0.6, Glut-$1^{+/-}$ 64 ± 3; WT 72 ± 13) or cerebellum (P=0.7, Glut-$1^{+/-}$ 1174 ± 85; WT 1245 ± 147). At P21, the stereological quantification showed equal neuron numbers and densities in the cortical area (layers 1-6) between Glut-$1^{+/-}$ and WT (P=0.4, Glut-$1^{+/-}$ 17000 ± 1159 (mean ±SEM), CE 0.03, WT 15668 ± 923, CE 0.03; density P=0.5, Glut-$1^{+/-}$ 7378 ± 455 (mean per 10^3 μm^2 ±SEM), WT 7708 ± 189) Also, at P21, there were no quantitative differences in the neuron numbers or densities of the hippocampal CA1 pyramidal neurons (P=0.7, Glut-$1^{+/-}$ 51020 ± 2373, CE 0.06; WT 52260 ± 1776, CE 0.05) or dentate gyrus granular cells between Glut-$1^{+/-}$ and WT (P=0.8, Glut-$1^{+/-}$ 95904 ± 6523, CE 0.04; WT 94104 ± 4780, CE 0.04; densities: CA1: P=0.4, Glut-$1^{+/-}$ 7007 ± 1476 (mean per 10^3 μm^2 ±SEM), WT 5518 ± 700; dentate gyrus: P= 0.5, Glut-$1^{+/-}$ 10530 ± 1377, WT 9333 ± 390). The analysis of cortex and hippocampus of mature animals (14-24 months) showed a decreasing trend in cell numbers in Glut-$1^{+/-}$ mice for the dentate gyrus and CA1 compared to WT (Figure 2.) (CA1: P=0.2, Glut-$1^{+/-}$ 43141 ± 2486 (mean ±SEM), CE 0.05, Wt 47835 ± 2140, CE 0.05; density P=0.4, Glut-$1^{+/-}$ 6415 ± 621 (mean per 10^3 μm^2 ±SEM), WT 5674 ± 580; DG: P=0.6, Glut-$1^{+/-}$ 90638 ± 7957 (mean ±SEM), CE 0.05, Wt 95319 ± 4807, CE 0.05; density P=0.5, Glut-$1^{+/-}$ 11553 ± 306 (mean per 10^3 μm^2 ±SEM), WT 12368 ± 1059). The cortical neuron numbers (layers 1-6) and densities were the same in mature Glut-$1^{+/-}$ mice compared to WT (P=1.0, Glut-$1^{+/-}$ 29576 ± 1772 (mean ±SEM), CE 0.03, WT 29568 ± 2028, CE 0.03; density P=0.5, Glut-$1^{+/-}$ 1728 ± 65 (mean per 10^3 μm^2 ±SEM), WT 1615 ± 131).

Proliferation

We analyzed the cerebrum and the cerebellum with two markers of proliferation: phospho-H3 staining and BrdU uptake. There were no apparent differences in developmental proliferation between Glut-$1^{+/-}$ and WT at ages P2, P7, P10 or P12, and equal proliferation was present in the dentate gyrus and subventricular zones at ages P60 and P90. At P10, the proliferation rate was not decreased in the Glut-$1^{+/-}$ cerebellum (group mean ± SEM) (P=0.6, Glut-$1^{+/-}$ 347 ± 44; WT 317 ± 38) by phospho-H3 histochemistry quantification. In addition, BrDU quantification showed equal cortical proliferation rate at P10 between Glut-$1^{+/-}$ and WT (P= 0.6, Glut-$1^{+/-}$ 293 ± 47; WT 333 ± 58).

Neuron size

We analyzed cell size both on histological sections as well as in sections stained for neuronal markers. The neuron size was unaffected at all ages (H&E, Nissl), from newborns to mature animals. The quantification of SMI-311 stained neurons, at 3 months of age, when both the brain growth deceleration and reactive astrocytosis had stabilized, showed no differences in neuron size (mean area in pixels ± SEM, 100 pixels ~1.7 μm^2) in somatosensory cortex layer 2-3 (P=0.5, Glut-$1^{+/-}$ 914 ± 51; WT 861 ± 50), layer 5 (P=0.9, Glut-$1^{+/-}$ 1177 ± 21; WT 1182 ± 50), or piriform cortex between Glut-$1^{+/-}$ and WT (P=0.8, Glut-$1^{+/-}$ 1264 ± 139; WT 1218 ± 112). These findings were supported by the lack of mTOR-pathway activation at this age in Glut-$1^{+/-}$ vs. WT, a key regulator of cell size, in the Glut-$1^{+/-}$ mice (see below).

Dendritic compartment

Under some pathological conditions, cell body size is unaffected but a decrease in neurite arbors may correlate with micrencephaly. Therefore, we investigated dendritic arborization in Glut-$1^{+/-}$ mice. SMI-32 and MAP2 dendritic staining were equal in Glut-$1^{+/-}$ mice, compared to the WT. Golgi-Cox quantification of proximal and distal dendritic branches showed no

significant changes in dendritic arborization in somatosensory cortex in Glut-1$^{+/-}$ mice (proximal branches: P= 0.14, Glut$^{+/-}$ 9 ± 2, WT 8 ± 1; distal branches: P= 0.92, Glut$^{+/-}$ 13 ± 2, WT 13 ± 2; mean ± SD). Visualization by Golgi-Cox staining did not show differences in dendritic spine numbers or morphology in cortex or hippocampus, between Glut-1$^{+/-}$ and WT. Finally, we assessed the synaptic portion of the neuropil by western blotting for synaptic proteins. Presynaptic protein synapsin-1 and postsynaptic protein PSD-95 were unaffected in adult Glut-1$^{+/-}$ mice (N=7, ea. group). Together these results indicate that the neuritic arbors, dendritic spines and synapses are not measurably reduced in the micrencephalic Glut-1$^{+/-}$ mice.

Astrocyte activation

Increased reactive astrocytosis (GFAP) was found in all mature Glut-1$^{+/-}$ mice. GFAP-positive astrocytes extended to the deeper cortical layers in the Glut-1$^{+/-}$ mice, compared to the WT mice, which contained only a few GFAP-positive astrocytes in layers 1 and 2. Also, increased thalamic astrocytosis was present in Glut-1$^{+/-}$ mice. (Figure 3.) Other cerebral areas, or cerebellum, did not show distinct differences in astrocyte activation. Morphologically, reactive astrocytes showed increased number and thickness of the processes in Glut-1$^{+/-}$ mice. Quantification confirmed a significant increase in GFAP staining by P21 (somatosensory cortex layer 1-3, P=0.01; piriform cortex, P=0.001). The astrocyte reactivity increased as the animals matured (at 3 months: somatosensory cortex layer 1-3, P=0.001, piriform cortex, P=0.007), and then plateaued. (Figure 4.) Cortical astrocyte proliferation was not found (phospho-Histone-3/ BrDU, at ages P30, P60, or P90).

mTOR-pathway

Since the TSC/mTOR-pathway is a critical regulator of cellular energy metabolism and cellular stress responses, we investigated whether this pathway was affected in Glut-1$^{+/-}$ brain samples from suckling pups (P7 and P14), and from mature mice (3-6 month). In the suckling Glut-1$^{+/-}$ pups, the mTOR-pathway was not affected at age P7 (P-mTOR P=0.25, P-GSK3-β P=0.9, P-Akt P=0.6, P-ACC P=0.6, P-S6: P=0.3), but at age P14, P-mTOR was significantly elevated (P=0.01), and P-GSK3-β was significantly reduced (P=0.05) compared to WT (P-Akt P=0.5, P-ACC P=0.2, P-S6: P=0.15). (Figure 5.) In the mature mice, the mTOR-pathway was not significantly affected in the resting state, between Glut-1$^{+/-}$ and WT. After six hours of fasting, a trend for enhanced inhibition of glycogen synthesis by P-GSK3-β (P=0.07) was detected in the Glut-1$^{+/-}$ female group (4 of 5 females; males unaffected) by western blot. A less striking trend for increase was evident in the female Glut-1$^{+/-}$ group for P-Akt-1 (P=0.18), and P-ACC (P=0.13, fatty acid oxidation). (Figure 5.) One of five fasted female Glut-1$^{+/-}$ animals showed clearly increased P-S6 activation on histochemistry, compared to WT female animals. There were no differences in P-S6 staining in any of the fasted Glut-1$^{+/-}$ male animals (N=4). Histological quantification of P-S6 revealed no significant differences between fasted Glut-1$^{+/-}$ and WT female groups (P=0.63, Glut-1$^{+/-}$ 357 ± 105; WT 283 ± 69, group mean ± SEM). Also, in western blotting analysis, the P-S6 was not significantly changed in either female (P=0.4) or male (P=1.0) Glut-1$^{+/-}$ animals. (Figure 6.)

Lithium Chloride studies

We noted that P-GSK3-β was perturbed in the developing Glut-1$^{+/-}$ mice, as well as in fasting Glut-1$^{+/-}$ mice. Therefore, we investigated the effect of the GSK3-β inhibitor lithium chloride (20mM, 24h) on skin fibroblast cultures from Glut-1 DS patients (N=5), and healthy controls (N=3). Before treatment, the baseline mean glucose uptake in Glut-1 DS group was 66% of the controls (glucose uptake fmol/min/mg prot. ± SEM: Glut-1 DS group 3240 ± 965, control group 4916 ± 907). The mean glucose uptake increased significantly (45%) after lithium chloride treatment (20mM, 24 h) in both groups, (glucose uptake fmol/min/mg prot. ± SEM:

Glut-1 DS group 4508 ± 1212, control group 7168 ± 1238) (Glut1 DS P=0.007, controls P=0.03). (Figure 7.)

DISCUSSION

Postnatal brain growth deceleration (acquired microcephaly), a clinical signature of patients with Glut-1 DS, also is a prominent feature of murine Glut-1 deficiency. In our prior studies, the mature Glut-$1^{+/-}$ mice brain weights were about 8 % smaller than the WT (Wang et al., 2006). The current study documents normal brain weight at birth and post-natal deceleration of brain weight that is increasingly evident after age P10 and statistically significant (P>0.001) by the end of the suckling period (P21). Thereafter, the discrepancy (7-8%) between the two groups remains constant, when the glucose metabolic demands have receded from the higher developmental values to the lower mature values.

The mouse brain normally undergoes substantial apoptosis during pre-natal growth and development and during the postnatal period before weaning. (Blaschke et al., 1996; Thomaidou et al., 1997) The postnatal brain growth spurt is also the time for active synaptogenesis. (Gohlke et al., 2004) In our studies, the postnatal cerebral and cerebellar developmental apoptosis and proliferation were not significantly affected in the Glut-$1^{+/-}$ mouse. We did not detect changes in hippocampal or cortical neuron numbers or densities at weaning (P21), when significant micrencephaly was present. The volumetric analysis of mature mice showed a significant decrease in total hippocampal volume, and a corresponding trend for decreased total forebrain and cerebellum volume. The lower estimated neuron numbers in mature Glut-$1^{+/-}$ mouse hippocampus were not significant. The documented structural changes of the Glut-$1^{+/-}$ mouse brain are subtle, and perhaps uniformly or regionally distributed, thereby escaping more robust detection by the methods that we employed in this study. Importantly, the experimental findings are in agreement with our observations in the human condition. Glut-1 deficient patients have significant functional disturbances with minimal structural alterations. Head growth deceleration and acquired microcephaly is a common feature, and the functional disturbances are disproportionate. We view these subtle structural changes as the minimal anatomical expression of chronic nutrient deficiency during this critical period of neurological development. The functional consequences are substantially greater. Our studies also indicate that the superimposed effects of aging on the hippocampus of Glut-$1^{+/-}$ mice deserve further investigation.

Alternate fuel sources also may provide some protection to the developing brain. A significant fraction of cerebral energy needs during post-natal development is met by utilization of ketone bodies (β-hydroxybutyrate and acetoacetate) (Owen et al. 1967; De Vivo et al. 1978). Rodent milk is high in fat content peaking at P14, (Gors et al., 2009) and contributing to hepatic ketogenesis in the nursing pups. Ketone bodies are transported across the BBB via monocarboxylate transporters (MCT1) (Pellerin et al., 1998; Pierre and Pellerin, 2005). MCT transporters are present at the late embryonic stage, peak post-natally by P15 mid-way through the suckling period, and decline to the mature levels by weaning. (Vannucci and Simpson, 2003; Baud et al., 2003). This profile corresponds with the period of maximal metabolic stress when we first note deceleration of brain weight and emergence of reactive astrocytosis. Breastfeeding may be neuroprotective during this critical period of brain development by increasing the availability of alternate fuel sources for brain metabolism. Our analysis of the mTOR-pathway during postnatal brain development did not show obvious signs of energy deprivation at ages P7 or P14 in the Glut-$1^{+/-}$ mice. However, P-mTOR was significantly elevated at P14, possibly an attempt to enhance Glut-1 transporter activity during this crucial growth period, especially since MCT transporter activity is declining in the P15-21 period during the weaning process.

GSK3-β (glycogen synthase kinase) is an enzyme that is important during development. (Zhou F.Q. et al., 2004) The phosphorylated inactive form, P-GSK3-β, is capable of inhibiting apoptosis in the setting of energy failure, and of regulating cell structure through microtubule-associated proteins (Beurel E, 2006). At P14, during the peak of postnatal brain development, P-GSK3-β was significantly decreased in the Glut-$1^{+/-}$ mice, in the absence of changes in total GSK3-β. The implications of this relative imbalance in active/ inactive forms of GSK3-β in the developing Glut-$1^{+/-}$ mice, compared to WT, remains unclear, but it may be related to the development of the micrencephaly in these mice.

GSK3-β overexpression reduces Glut-1 transporter expression and glucose uptake via mTOR-pathway in vitro (Buller et al., 2008). Spittaels et al. (2002) described a transgenic mouse overexpressing constitutively active GSK3-β. The neuropathological correlates were profound with diffuse micrencephaly (ca. 20% reduction in brain weight), normal cortical layering (in the absence of apoptosis), reduced cortical somatodendritic compartment manifested as reduced neuron size, reduced thickness of dendrites (SMI-32), and diminished MAP2 (microtubule-associated protein). The Glut-$1^{+/-}$ mouse changes are more subtle with about 6-8 % reduction in brain weight compared to WT. We detected no significant differences in neuron size, dendritic thickness, or cortical thickness.

The mTOR signaling pathway was not obviously affected in the mature Glut-$1^{+/-}$ mice. When mature mice were exposed to six-hours of fasting, we detected a trend for elevated P-GSK3-β^{Ser9} (glycogen synthesis inhibition) only in the female Glut-$1^{+/-}$ mice. In addition to P-GSK3-β, its upstream modulator P-Akt, and P-ACC were elevated (trend) in the fasting state. Fasting did not induce any other discernable mTOR-pathway changes in the adult Glut-$1^{+/-}$ mouse. Buller et al. (2008) reported that GSK3-β inhibition increased Glut-1 activity in murine cell cultures. In our experiments with Glut-1 deficient human skin fibroblast cultures, acute treatment (20mM, 24h) with the GSK3-β inhibitor lithium chloride increased glucose uptake in both Glut-1 DS patient cells, as well as in healthy control cells (group mean ~45%, range 10-90%). Our data, in the aggregate, suggest that GSK3-β inhibition may be protective in Glut-1 deficiency, and deserves further investigation as a therapeutic intervention.

Significant reactive astrocytosis emerged in cortex and thalamus by weaning (P21), which further intensified (in the absence of signs for astrocyte proliferation) until P90 before plateauing. The emergence of reactive astrogliosis coincides with brain weight deceleration, and continues to increase after the brain weight has stabilized suggesting continuing metabolic stress to the mature brain. Similar neonatal cortical astrogliosis has been reported in mice exposed to neonatal MCT transport blockade by CIN (alpha-cyano-4-hydroxycinnamate), simulating brain nutrient deficiency by limiting the supply of organic acids (ketone bodies, lactate and pyruvate) during this critical period of brain development. (Adle-Biassette et al., 2007) The MCT-blockade did not enhance cortical apoptosis, an observation that is congruent with our findings in the Glut-1 deficient mouse model. Three-day treatment (P1-P3) with CIN, however, disrupted cortical neuronal migration. This finding suggests the possibility that ketone bodies may be a more critical fuel source for these neurodevelopmental events. In our study, we did not explore the cortical neuronal migration patterns in the Glut-$1^{+/-}$ mouse, but cortical layering, neuron numbers and density were normal in young and mature mice.

In the mature Glut-$1^{+/-}$ mouse, which exhibits about 35-50% reduction of Glut-1 compared to WT, there were no detectable histopathological changes, no enhanced apoptosis, or cell size changes. The Glut-$1^{+/-}$ mouse also presents with electrographic seizure activity (previously reported by Wang et al., 2006), which is an additional metabolic stressor in the already energy-compromised brain and may cause excitotoxic injury and cell loss especially in the seizure sensitive hippocampus. (Holmes et al., 2002) Astrocyte reactivity has been reported to increase after seizure activity (Shapiro et al., 2008), and synaptic proteins may also be affected by

epileptic activity (Jiang et al., 2007; Wyneken et al., 2001). In the adult Glut-$1^{+/-}$ mouse, the reactive astrogliosis increased until adulthood (3 months), a sign of continuing metabolic stress and/ or seizure activity. No changes in neuropil structure or synaptic proteins (PSD-95, synapsin-1) were detectable in the adult Glut-$1^{+/-}$ mice. The total hippocampal volume was decreased in mature Glut-$1^{+/-}$ mice, and we noted a subtle non-significant decrease in hippocampal neuron number in the mature mice (18 months). The chronic metabolic compromise and/or seizure activity may produce incremental structural damage in the hippocampus over the lifespan of the Glut-$1^{+/-}$ mouse, as reflected in the demonstrated volume loss.

In summary, the heterozygous Glut-1 mouse model demonstrates subtle but definite clinical and neuropathological findings. The earliest findings are decreased brain weight and reactive astrocytosis. These findings could not be explained by enhanced apoptosis. Our investigative methods may not have been adequately sensitive to detect minimal change in these pathways. Alternatively, there may be other mechanisms at play that compromise organ structure and function during chronic subtle cellular energy compromise. The genetic background (129S6/SvEvTac) of our Glut-$1^{+/-}$ mouse model also may have muted the neurochemical response to the metabolic stress thereby mitigating the clinical phenotype. It is known that pathogenic mutations placed in this genetic background are associated with milder clinical phenotypes (Sheldon et al., 1998). Further studies are planned to investigate the role of GSK3-β in the regulation of GLUT1, to modify the genetic background and increase the phenotypic severity, and to impose additional environmental stressors on the chronic nutrient deficiency in an effort to ferret out other molecular and cellular mechanisms that modify the clinico-pathological consequences of GLUT1 haploinsufficiency.

Acknowledgments

These studies were supported by USPHS grants 5K12-NS01698 (DCD/PMU) and 5RO1NS37949 (DCD) and by support from the Colleen Giblin and Will Foundations (DCD). We thank Prof. Serge Przedborski and Scott Small for helpful comments, and access to their laboratory facilities. We are also grateful to Dr. Phyllis Faust for histological advice, and Vernice Jackson-Lewis, Marcela Assanah, Suzy Alexander, and Alexander Kushnir for their technical guidance, as well as Dalina Stiner and Leslie Bagay for their technical assistance.

REFERENCES

Adle-Biassette H, Olivier P, Verney C, Fontaine RH, Evrard P, Henin D, Massias L, Gressens P, Baud O. Cortical consequences of in vivo blockade of monocarboxylate transport during brain development in mice. Ped. Res 2007;61(1):54–60.

Baud O, Fayol L, Gressens P, Pellerin L, Magistretti P, Evrard P, Verney C. Perinatal and early postnatal changes in the expression of monocarboxylate transporters MCT1 and MCT2 in the rat forebrain. J. Comp. Neurol 2004;465:445–454. [PubMed: 12966567]

Beurel E, Jope RS. The paradoxical pro- and anti-apoptotic actions of GSK3 in the intrinsic and extrinsic apoptosis signaling pathways. Prog. Neurobiol 2006;79(4):173–189. [PubMed: 16935409]

Blaschke AJ, Staley K, Chun J. Widespread programmed cell death in proliferative and postmitotic regions of the fetal cerebral cortex. Development 1996;122:1165–1174. [PubMed: 8620843]

Buller CL, Loberg RD, Fan M-H, Zhu Q, Park JL, Vesely E, Inoki K, Guan K-L, Brosius FC III. A GSK-3/TSC2/mTOR pathway regulates glucose uptake and GLUT1 glucose transporter expression. Am. J. Physiol. Cell Physiol 2008;295:C836–C843. [PubMed: 18650261]

Chi MM-Y, Pingsterhaus J, Caraynnopoulos M, Moley KH. Decreased glucose transporter expression triggers BAX-dependent apoptosis in the murine blastocyst. J. Biol. Chem 2000;275(51):40252–40257. [PubMed: 10995754]

Daneman R, Agalliu D, Zhou L, Kuhnert F, Kuo CJ, Barres BS. Wnt/b-catenin signaling is required for CNS, but not non-CNS, angiogenesis. PNAS 2009;106(2):641–646. [PubMed: 19129494]

De Vivo DC, Trifletti RR, Jacobson RI, Ronen GN, Behmand RA, Harik SA. Defective glucose transport across the blood-brain barrier as a cause of persistent hypoglycorrhachia, seizures, and developmental delay. N. Eng. J. Med 1991;325:51–56.

De Vivo DC, Leckie MP, Ferrendelli JS, McDougal DB Jr. Chronic Ketosis and Cerebral Metabolism. Ann. Neurol 1978;3:331–337. [PubMed: 666275]

Endo H, Nito C, Kamada H, Noshi T, Chan PH. Activation of the Akt/GSK3b signaling pathway mediates survival of vulnerable hippocampal neurons after transient global cerebral ischemia in rats. J. Cerebral Blood Flow & Metabolism 2006;26:1479–1489.

Frame S, Cohen P. Review article: GSK3 takes centre stage more than 20 years after its discovery. Biochem. J 2001;359:1–16. [PubMed: 11563964]

Gors S, Kucia m. Langhammer M, Junghans P, Metges CC. Technical Note: Milk composition in mice – Methodological aspects and effects of mouse strain and lactation day. J. Dairy Sci 2009;92:632–637. [PubMed: 19164675]

Gohlke JM, Griggith WC, Faustman EM. The role of cell death during neocortical neurogenesis and synaptogenesis: implications from a computational model for the rat and mouse. Devel. Brain Res 2004;151:43–54. [PubMed: 15246691]

Hammerman PS, Fox CJ, Thompson CB. Beginnings of a signal-transduction pathway for bioenergetic control of cell survival. Trends in Biochem. Sciences 2004;29(11):586–592.

Hay N, Sonenberg N. Review: Upstream and downstream of mTOR. Genes & Devel 2004;18:1926–1945. [PubMed: 15314020]

Heilig CW, Saunders T, Brosius FC III, Moley K, Heilig K, Baggs R, Guo LR, Conner D. Glucose transporter-1-deficient mice exhibit impaired development and deformities that are similar to diabetic embryopathy. PNAS 2003;100(26):15613–15618. [PubMed: 14673082]

Hogan A, Heyner S, Charron MJ, Copelabd NG, Gilbert DJ, Jenkins NA, Thorens B, Schultz GA. Glucose transporter gene expression in early mouse embryos. Development 1991;113:363–372. [PubMed: 1765007]

Holmes GL. Animal-induced neuronal injury: Animal data. Neurology 2002;59(suppl. 5):S3–S6. [PubMed: 12428025]

Jensen PJ, Gitlin JD, Carayannopoulos MO. Glut1 deficiency links nutrient availability and apoptosis during embryonic development. JBC 2006;281(19):13382–13387.

Jiang Q, Wang J, Wu X, Jiang Y. Alterations of NR2B and PSD-95 expression after early-life epileptiform discharges in developing neurons. Int. J. Devl. Neuroscience 2007;25:165–170.

Khan JY, Rajakumar RA, MCKnight RA, Devaskar UP, Devaskar SU. Developmental regulation of genes mediating murine brain glucose uptake. Am. J. Physiol 1999;273(3Pt2):R892–900. [PubMed: 10070152]

Maher F, Vannucci SJ, Simpson IA. Glucose transporter proteins in brain. FASEB J 1994;8:1003–1011. [PubMed: 7926364]

Owen OE, Morgan AP, Kemp HG, Sullivan JM, Herrera MG, Cahill GF Jr. Brain Metabolism during Fasting. J. Clin. Inv 1967;46(10):1589–1595.

Pellerin L, Pellegri G, Martin J-L, Magistretti PJ. Expression of monocarboxylate transporter mRNAs in mouse brain: Support for a distinct role of lactate as an energy substrate for the neonatal vs. adult brain. Neurobiology 1998;95:3990–3995. Physiol. Regulatory Integrative Comp. Physiol. 276, 892-900.

Pierre K, Pellerin L. Monocarboxylate transporters in the central nervous system: distribution, regulation and function. J. Neurochem 2005;94:1–14. [PubMed: 15953344]

Ramamurthy S, Ronnett GV. Developing a head for energy sensing: AMP-activated protein kinase as a multifunctional metabolic sensor in the brain. J. Physiol 2006;574(1):85–93. [PubMed: 16690704]

Shapiro LA, Wang L, Ribak CE. Rapid astrocyte and microglial activation following pilocarpine induced seizures in rats. Epilepsia 2008;49(Suppl. 2):33–41. [PubMed: 18226170]

Sheldon RA, Sedik C, Ferriero DM. Strain-related brain injury in neonatal mice subjected to hypoxia–ischemia. Brain Research 1998;810:114–122. [PubMed: 9813271]

Spittaels K, Van Den Haute C, Van Dorpe J, Terwel D, Vandezande K, Lasrado R, Bruynseels K, Irizarry M, Verhoye M, Van Lint J, Vanderheede JR, Ashton D, Mercken M, Loos R, Hyman B, Van Der Linden A, Geerts H, Van Leuven F. Neonatal neuronal overexpression of glycogen synthase

kinase-3B reduces brain size in transgenic mice. Neuroscience 2002;113(4):797–808. [PubMed: 12182887]

Steinberg GR, Macaulay SL, Febbraio MA, Kemp BE. Review: AMP-activated protein kinase – the fat controller of the energy railroad. Can. J. Physiol. Pharmacol 2006;84:655–665. [PubMed: 16998529]

Thomaidou D, Mione MC, Cavanagh JFR, Parnavelas JG. Apoptosis and its relation to the cell cycle in the developing cerebral cortex. J. Neurosci 1997;17(3):1075–1085. [PubMed: 8994062]

Vannucci SJ, Simpson IA. Developmental switch in brain nutrient transporter expression in the rat. Am. J. Physiol. Endocrinol. Metab 2003;285:E1127–E1134. [PubMed: 14534079]

Wang D, Pascual JM, Yang H, Engelstad K, Jhung S, Sun RP, De Vivo DC. Glut-1 Deficiency Syndrome: Clinical, Genetic, and Therapeutic Aspects. Ann. Neurol 2005;57:111–118. [PubMed: 15622525]

Wang D, Pascual JM, Yang H, Engelstad K, Mao X, Cheng J, Yoo J, Noebels JL, De Vivo DC. A mouse model for Glut-1 haploinsufficiency. Human Mol. Gen 2006;7:1169–1179.

West JW. Stereological methods for estimating the total number of neurons and synapses: issues of precision and bias. Trends Neurosci 1999;22:51–61. [PubMed: 10092043]

Wieman HL, Wofford JA, Rathmell JC. Cytokine stimulation promotes glucose uptake via phosphatidylinositol-3 kinase/Akt regulation of Glut1 activity and trafficking. Molecular Biology of the Cell 2007;18:1437–1446. [PubMed: 17301289]

Wyneken U, Smalla K-H, Marengo JJ, Soto D, De La Cerda A, Tischmeyer W, Grimm R, Boeckers TM, Wolf G, Orrego F, Gundelfinger ED. Kainate-induced seizures alter protein composition and N-methyl-D-aspartate receptor function of rat forebrain postsynaptic densities. Neuroscience 2001;102:65–74. [PubMed: 11226670]

Yang Q, Guan K-L. Expanding mTOR signaling. Cell Res 2007;17:666–681. [PubMed: 17680028]

Yushkevich PA, Piven J, Hazlett HC, Smith RG, Ho S, Gee JC, Gerig G. User-guided 3D active contour segmentation of anatomical structures, significantly improved efficiency and reliability. Neuroimage 2006;31(3):1116–28. [PubMed: 16545965]

Zhou FQ, Zhou J, Dedhar S, Wu Y-H, Snider WD. NGF-Induced Axon Growth Is Mediated by Localized Inactivation of GSK-3 and Functions of the Microtubule Plus End Binding Protein APC. Neuron 2004;42:897–912. [PubMed: 15207235]

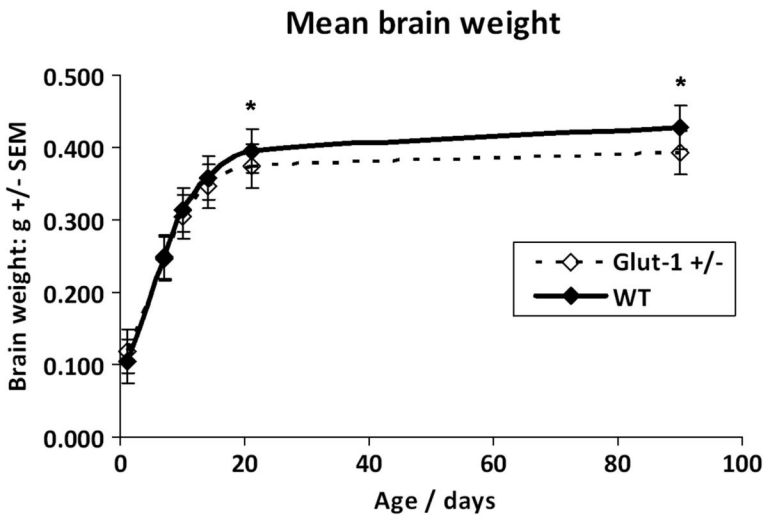

Figure 1.

Glut-$1^{+/-}$ mouse brain growth deceleration is evident after P7. Statistically significant deceleration of brain growth appears by weaning age P21 (*P=0.001). The brain weight difference between WT and Glut-1 +/− is constant after P21.

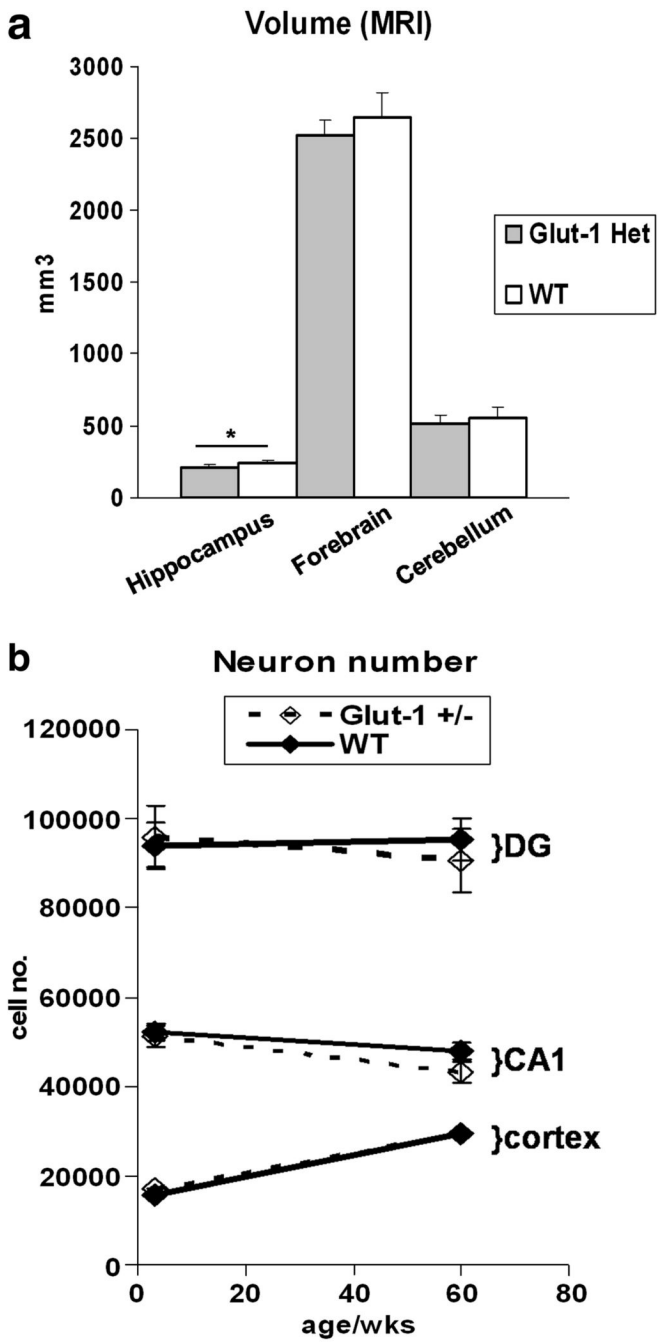

Figure 2.

MRI volumetric analysis of mature Glut-$1^{+/-}$ and WT mice (mean age: 17 months) showed significant reduction of total hippocampus volume in Glut-$1^{+/-}$ (*P=0.02), and a trend for volumes of total forebrain (P=0.12), and cerebellum (P=0.28). Stereological neuron quantification at P21 and in mature mice (comparable to the MRI study) detected a downward trend in the hippocampus neuron numbers (CA1, dentate gyrus) in mature Glut-$1^{+/-}$ mice. Cortical neuron numbers (layers 1-6) were the same at P21 or in mature Glut-$1^{+/-}$ mice.

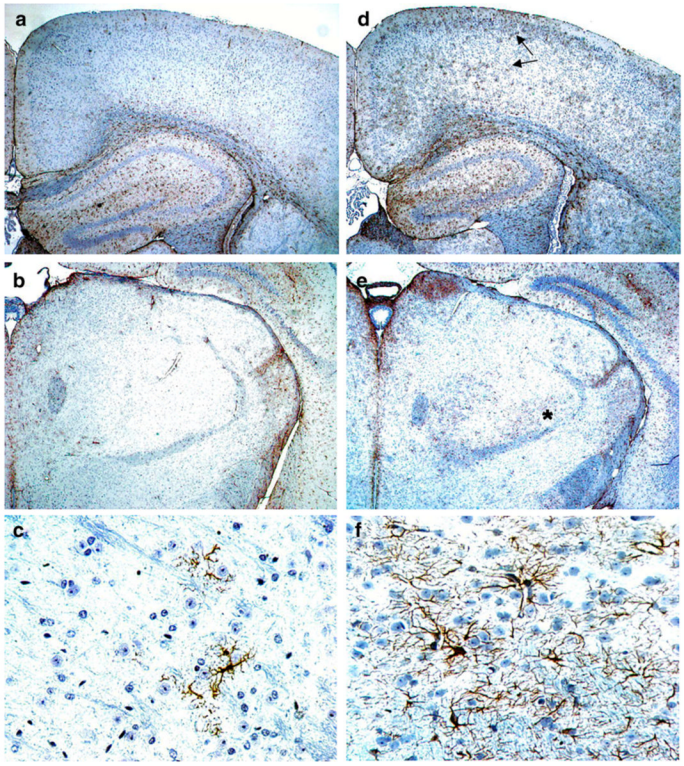

Figure 3.
GFAP staining in adult (P90) WT (A.-C.) and Glut-1$^{+/-}$ mice (D.-F.). Glut-1$^{+/-}$ mouse brain shows enhanced GFAP staining of astrocytes, compared to WT. Increased reactive astrocytosis is prominent in both superficial and deeper layers of Glut-1$^{+/-}$ mouse cortex (D., arrows), and thalamus (E., asterisk). The Glut-1$^{+/-}$ mouse thalamic reactive astrocytes (F.) have abundant astrocytic processes, compared to WT thalamus (C.). (A/B/D/E, 4X magnification, C/F, 40X magnification)

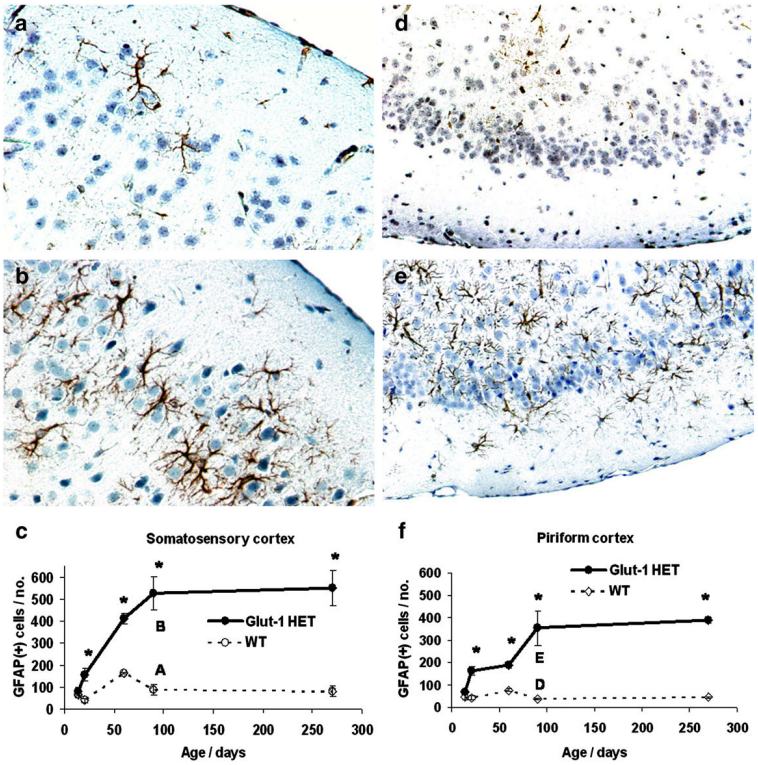

Figure 4.

GFAP staining in adult (P90) WT (A./D.) and Glut-$1^{+/-}$ mice (B./E.). The reactive astrocytosis (GFAP) of Glut-$1^{+/-}$ mouse somatosensory cortex (B.) becomes significantly increased by P21 (C.) compared to WT. (Respective images at P90: A./B.) Similarly, reactive astrocytosis becomes significantly increased in piriform cortex of Glut-$1^{+/-}$ mouse by P21 (F.), compared to WT. (Respective images at P90: D./E.) The reactive astrocytosis continues to progress until P90. (A./B., 40X magnification; D./E., 20X magnification.) (*P<0.01)

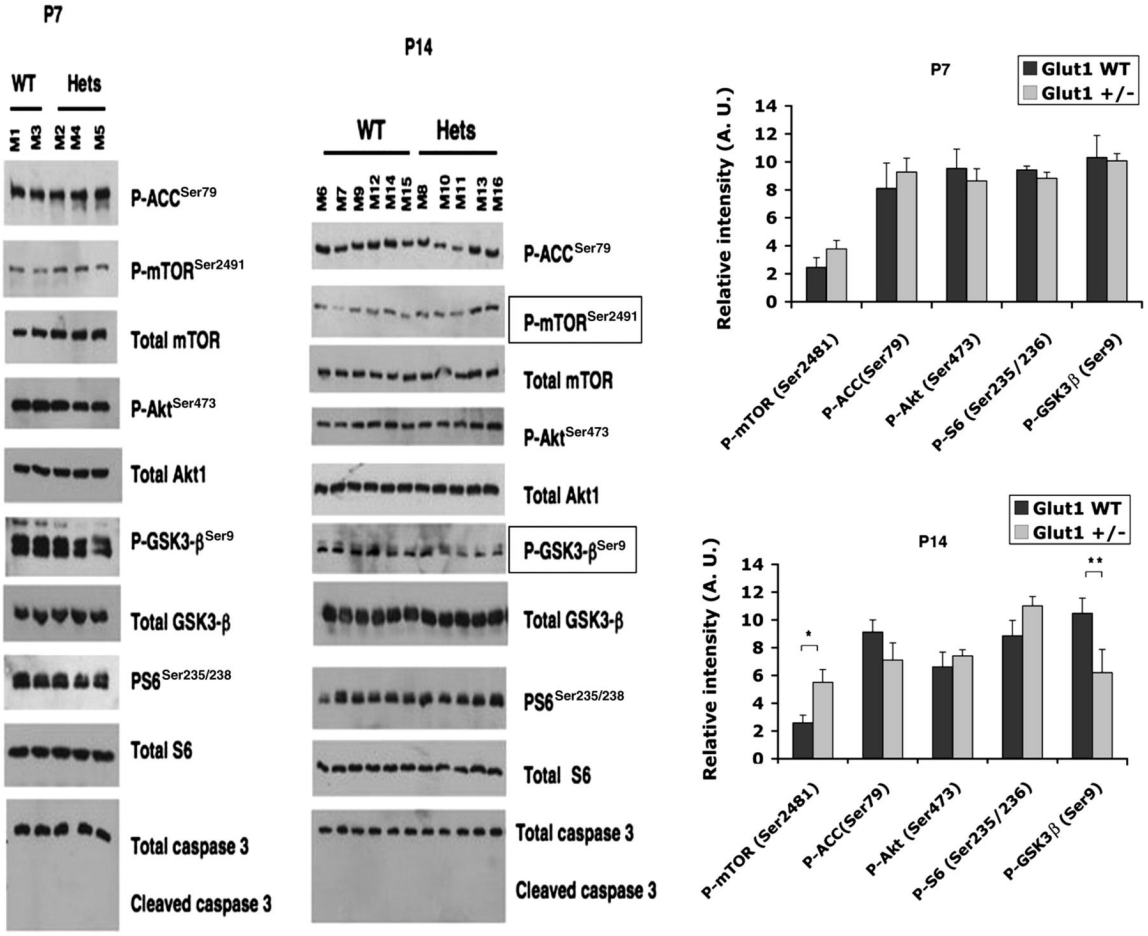

Figure 5.

The mTOR-pathway was not significantly affected at P7 (P-mTOR, P=0.25; P-GSK3-β, P=0.9; P-Akt, P=0.6; P-ACC, P=0.6; P-S6, P=0.3). At P14, P-mTOR was significantly elevated (*P=0.01), and P-GSK3-β significantly decreased (**P=0.05) in Glut-$1^{+/-}$ mice. (P-ACC, P=0.2; P-Akt, P=0.5; P-S6, P=0.15). Cleaved caspase-3 (apoptosis) was not elevated in Glut-$1^{+/-}$ mice.

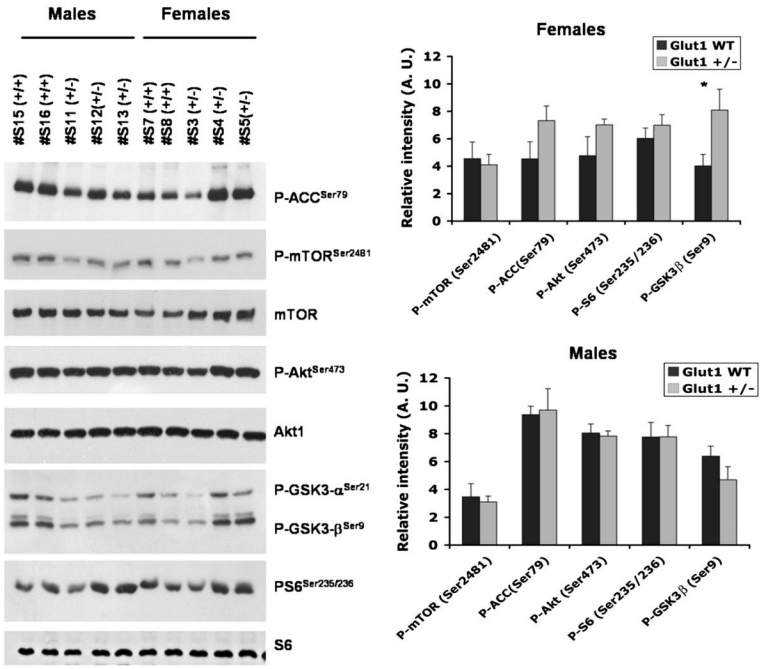

Figure 6.

Mature (P90-180) female (N= 4-5 ea. group) and male mice (N=5-6 ea. group) were fasted for 6 hours. The female Glut-$1^{+/-}$ mice showed a trend for increased P-GSK3-β (*P=0.07), P-ACC (P=0.13) and P-Akt (P=0.18) (P-mTOR, P=0.8; P-S6, P=0.2). The mTOR-pathway was the unaffected in male Glut-$1^{+/-}$ mice.

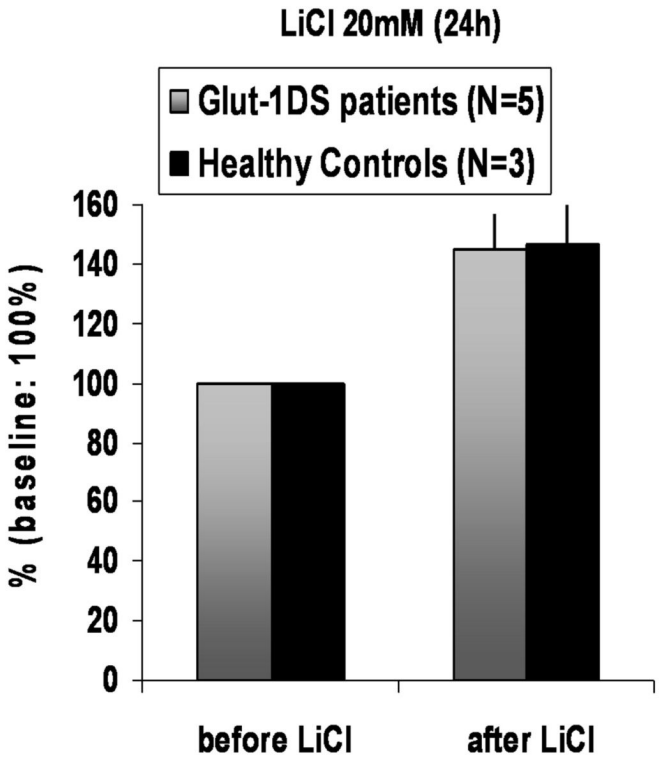

Figure 7.

Human cultured fibroblasts were treated with 20mM lithium chloride for 24 hours. The baseline (before treatment) mean glucose uptake in Glut-1 DS patient group was ~66% of the healthy controls. The mean increase in glucose uptake after treatment was increased by ~45% in the Glut-1 DS patient group (P=0.007, range in individual patients: 15-90%) and the healthy control group (P=0.03, range in individual healthy subjects: 30-70%). (Baseline mean glucose uptake without LiCl treatment in the control and $Glut^{+/-}$ cell lines set at 100%; uptake after LiCl treatment is expressed as % change +/−SEM.)

Neurobiol Dis. Author manuscript; available in PMC 2010 October 1.

Table 1

Body and brain weight of Glut-$1^{+/-}$ and WT mice at P7, P10, P14, P21, and P90-120. (Student's T-test)

AGE	Mouse	N	Brain weight (mg) mean +/− SD	Body weight (g) mean +/− SD	Brain P	Body P
P7	Glut-1 +/−	12	247 +/− 27	4.2 +/− 0.9	0.9	0.4
	WT	15	248 +/− 27	4.5 +/− 0.7		
P10	Glut-1 +/−	11	304 +/− 16	5.3 +/− 4.0	0.2	0.4
	WT	8	314 +/− 18	5.1 +/− 64		
P14	Glut-1 +/−	13	347 +/− 32	8.2 +/− 1.0	0.3	0.5
	WT	19	358 +/− 30	7.9 +/− 1.0		
P21	Glut-1 +/−	38	374 +/− 26	11.1 +/− 2.0	0.001*	0.2
	WT	35	398 +/− 33	11.4 +/− 1.9		
P90-120	Glut-1 +/−	20	394 +/− 27	23.6 +/− 4.5	0.001*	0.95
	WT	13	428 +/− 23	23.7 +/− 4.2		